Available online at www.sciencedirect.com

ScienceDirect

Proceedings of the Combustion Institute 37 (2019) 3109–3117

Proceedings of the Combustion Institute

www.elsevier.com/locate/proci

The role of local thermal non-equilibrium in modelling smouldering combustion of organic liquids

Marco A.B. Zanoni [a], José L. Torero [b], Jason I. Gerhard [a,*]

[a] *Department of Civil and Environmental Engineering, University of Western Ontario, London, ON N6A 5B9, Canada*
[b] *A. James Clark School of Engineering, The University of Maryland, College Park, MD 20742, USA*

Received 29 November 2017; accepted 28 May 2018
Available online 29 June 2018

Abstract

A one-dimensional numerical model of smouldering combustion was developed in order to better understand smouldering and accurately predict forced, upwards, self-sustained smouldering for the purposes of treating hydrocarbon-contaminated soil. The role of local thermal non-equilibrium was explored via a new heat transfer correlation obtained specifically for conditions typical of smouldering hydrocarbon-contaminated soil. The model was calibrated to a smouldering experiment and then confidence in the model was gained by independent simulations of additional experiments. The smouldering chemistry was represented by a two-step kinetic mechanism, with the results indicating that this simple framework was sufficient to reproduce the main features of self-sustained smouldering. Local thermal non-equilibrium was demonstrated to be significant in smouldering, with an average normalized temperature difference of 36% between the air and the sand/fuel. Moreover, incorporating the new non-equilibrium correlation provided accurate predictions, particularly in the heat transfer-dominated regions preceding and trailing the front. Results further demonstrated that the most widely used correlation in the literature effectively ensures local thermal equilibrium and such models could not reproduce the experiments.

Keywords: Smouldering combustion; Local thermal non-equilibrium; Interfacial heat transfer coefficient; Heat losses; Porous medium

1. Introduction

Smouldering combustion is a surface oxidation reaction common to porous organic solids [1]. Organic liquids embedded in an inert porous matrix can also smoulder due to the production of char during pyrolysis [2,3]. Soil is frequently contaminated by liquid hydrocarbons, such as bitumen, coal tar, and crude oil, and intentional smouldering is gaining acceptance as a soil remediation technology [4–6]. Numerical modelling of these smouldering processes is essential to determine operating conditions but simulating the intentional smouldering of liquids for remediation is challenging and novel. Models to date have either focused on porous organic solids [7,8] or have been heuristic

* Corresponding author.
E-mail address: jgerhard@uwo.ca (J.I. Gerhard).

https://doi.org/10.1016/j.proci.2018.05.177
1540-7489

Nomenclature

Latin Letters

A_s	surface area, m^2
C_p	specific heat capacity, J kg^{-1} K^{-1}
d_p	particle diameter, mm
h_m	mass transfer coefficient, kg m^{-2} s^{-1}
k	thermal conductivity, W m^{-1} K^{-1}
L	contaminated region length, m
P	pressure, Pa
R_g	ideal gas constant, J K^{-1} mol^{-1}
t_f	final Time, s
V	volume, m^3
Y	mass fraction

Subscripts/Superscript

b	bitumen
c	char
cl	cylinder
eff	effective
f	final
g	gas
0	initial
s	solid/bitumen
sp	sphere

engineering tools that significantly simplified chemical reactions and mass transfer processes [9,10].

Smouldering numerical models require appropriate chemistry. Smouldering kinetic mechanisms have received significant attention and been described with varying degrees of detail, from simple [11] to complex [8] and are typically presented as Arrhenius-type equations. The Arrhenius parameters – pre-exponential factor (A), activation energy (E), and heat of reaction (ΔH) – are obtained by analyzing Thermogravimetry (TG), Differential Thermogravimetry (DTG), and Differential Scanning Calorimetry (DSC) experiments on the fuel [1,7,12]. An analytical analysis [13] is useful for simple chemical schemes while complex schemes require stochastic methods such as Genetic Algorithms [7].

Smouldering numerical models also require appropriate heat transfer processes. In contrast to chemistry, heat transfer in smouldering has received little attention. Smouldering models treat heat transfer with one of two approaches [14]: Local Thermal Equilibrium (LTE) [11,15] and Local Thermal Non-Equilibrium (LTNE) [8,16]; the former assumes that the gas and the solid are in thermal equilibrium while the latter allows for heat exchange between them. There are numerous reasons to hypothesize that LTNE is important for simulating smouldering. Oliveira and Kaviany [14] note that highly exothermic reactions may cause LTNE. In addition, heat transfer (via convection and conduction) controls pyrolysis of the fuel ahead of the smouldering front and controls cooling of the hot, clean sand behind the front (heat is transferred to the cold air and is lost radially), with both affecting the energy balance at the reaction zone. Moreover, at high gas velocities smouldering can be extinguished by heat transfer processes [1,17].

LTNE models require an interfacial heat transfer coefficient (h_{sg}). This has been quantified via empirical Nusselt (Nu) versus Reynolds (Re) and Prandtl (Pr) numbers correlations [18, 19] that are not related to smouldering. For example, Wakao et al. [18]:

$$\mathrm{Nu} = \frac{h_{sg} d_p}{k_g} = 2 + 1.1\left(\mathrm{Re}^{0.6}\mathrm{Pr}^{1/3}\right) \quad (1)$$

is valid for $15 \leq \mathrm{Re} \leq 8500$, whereas natural and intentional smouldering typically exhibits $\mathrm{Re} < 15$. Nevertheless, Eq. (1) has been widely employed in smouldering numerical models, predicting large h_{sg} values [8], which may lead to the untested conclusion that the gas and solid are in thermal equilibrium in smouldering [16].

Recently, Zanoni et al. [19] used the convective propagation of a heat wave through sand (no smouldering) to develop a new correlation for h_{sg}:

$$\mathrm{Nu} = \frac{h_{sg} d_p}{k_g} = 0.001\left(\mathrm{Re}^{1.97}\mathrm{Pr}^{1/3}\right) \quad (2)$$

valid for $\mathrm{Pr} = 0.72$, $0.5 \leq \mathrm{Re} \leq 31$, and $0.125 < d_p < 2.000$ mm; these ranges are typical for smouldering remediation of liquids [6]. A recently developed criterion for the validity of assuming local thermal equilibrium was demonstrated to be violated within these parameter ranges, indicating that LTNE is appropriate and essential for heat transfer in these scenarios [19]. Heat generation and heat transfer parameters have the potential to compensate for errors when models are calibrated to experiments. Therefore, the minimum kinetic mechanisms necessary to simulate smouldering and the appropriate approach for heat transfer remain open questions.

The objective of this study was to develop and build confidence in a one-dimensional numerical model that simulates smouldering with explicitly quantified heat transfer. The target scenario was the intentional (forced), self-sustaining smouldering remediation of bitumen-contaminated sand. Simple smouldering chemistry (one pyrolysis and one oxidation reaction) was employed as a baseline scenario. The kinetic constants were populated from TG/DTG/DSC experiments. Only four independent parameters that minimize the potential for error compensation were calibrated to a base

Table 1
Smouldering experiments.

Exp. # [-]	u_g [a] [m s^{-1}]	Saturation (S_b) [-]	Repeats [-]	Air on (t_g) [s]	Heater off (t_h) [s]
1	0.058	0.15	3	4532 ± 378[b]	4865 ± 300[b]
2	0.025	0.15	1	4926	5357
3	0.050	0.15	1	5287	5670
4	0.083	0.15	1	5077	5329

[a] Volume per unit cross-sectional area per unit time.
[b] 95% confidence interval.

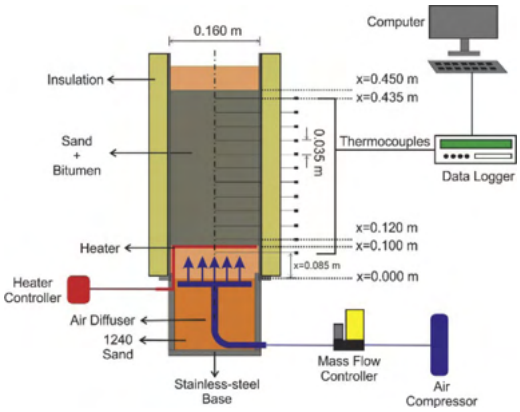

Fig. 1. Schematic of the experimental apparatus.

case smouldering experiment (conducted in triplicate). Confidence in the model was obtained by comparing predictions to observations of independent experiments. The role of heat transfer was analyzed by considering various LTE/LTNE models and comparing them to the experimental observations. This comparison provides unique conclusions about the importance and magnitude of LTNE in smouldering processes.

2. Methodology

2.1. Experiments

The smouldering experiments were carried out in a stainless-steel column (Fig. 1) following an established methodology [20]. A base case experiment (Exp. #1) was conducted in triplicate and another three experiments (Exp. #2–4) varied the injected Darcy air flux (u_g), Table 1.

The column contained 0.10 m of clean sand ($d_p = 0.88$ mm, particle density (ρ_s) = 2650 kg m^{-3}) below the heater and a 0.35 m layer (L) of a mixture (bulk density of 1726 kg m^{-3}) of sand and bitumen (density (ρ_b) = 1030 kg m^{-3}, PG 58-28, McAsphalt Industry Limited) above it. Eleven thermocouples spaced 0.035 m apart were assumed to measure the solid (sand/bitumen) temperature [19] along the column center-line every 2 s. Evaluating combustion only by thermocouple data is appropriated here, since the primary goal is to predict smouldering front propagation rates, peak temperatures, and temperature distributions. The apparatus was insulated with 5 cm of insulation (high-temperature mineral wool, McMaster-Carr) to minimize heat losses; under such conditions it is usually observed that approximately a 150 °C temperature drop occurs from the centreline to the wall, although radial temperatures were not measured in this case. Each experiment was initiated by powering the resistive heater until the temperature of the second thermocouple (the first in the bitumen, $x = 0.12$ m) reached 400 °C. Then, air injection at a fixed rate was supplied, which initiated smoldering. The heater was then switched off while the air was maintained. A self-sustained smouldering front propagated upwards until all the bitumen was consumed, leaving clean sand.

TG, DTG, and DSC experiments on the bitumen were conducted at heating rates (β) of 10, 20, 30, and 40 K min^{-1} under N_2 and air atmospheres. Since the DTG and DSC results (not shown) suggested two main decomposition peaks, one endothermic and one exothermic, a 2-step kinetic mechanism was proposed:

$$Bitumen \xrightarrow{R_b} v_c Char + (1 - v_c) Gas$$
$$Char + v_{O_2} O_2 \xrightarrow{R_c} Gas \quad (3)$$

Competing reactions are not considered since their influence on the observed smouldering behaviour is expected to be minor. Table 2 provides all determined values, including the reaction rates (R_i) described as first-order Arrhenius reactions, and the Arrhenius parameters (A_i and E_i) for each reaction (i) obtained by the use of Kissinger method [13,21]. Heat of reactions (ΔH_i) for pyrolysis and oxidation were determined from DSC experiments by the time integration of the heat flow over mass loss (mW mg^{-1}) under N_2 and air, respectively.

2.2. Modelling

A new, one-dimensional numerical model was developed in COMSOL Multiphysics (*Version 5.0*). The computational domain represents the 0.45 m sand/bitumen pack (Fig. 1). The model considers

Table 2
Kinetic parameters calculated by Kissinger method from TG and DSC experiments under N_2 and air at four heating rates (10, 20, 30, 40 K min^{-1}).

	N_2 (pyrolysis)				Air (oxidation)			
β [K min^{-1}]	T_p [K]	log (A_p) [log(s^{-1})]	E_p [kJ mol^{-1}]	ΔH_p [MJ kg^{-1}]	T_p [K]	log (A_c) [log(s^{-1})]	E_c [kJ mol^{-1}]	ΔH_c [MJ kg^{-1}]
10	725	7.5	135	1.62	848	3.0	90	−38.73
20	746				885			
30	758				921			
40	769				930			
	$R_b = A_b \exp(-\frac{E_b}{R_g T_s})(Y_b)$				$R_c = A_c \exp(-\frac{E_c}{R_g T_s})(Y_c)(Y_{O_2})$			

Table 3
Initial and boundary conditions for numerical model.

Eqs.	Initial condition	Boundary condition
(4)	$t = 0 \Rightarrow Y_b = 1;\ Y_c = 0$	-
(5)	$t = 0 \Rightarrow P_g = 101375$ Pa	$x = 0.00$ m $\Rightarrow \rho_g u_g = \rho_g u_g(t) \rightarrow \begin{cases} u_g(t) = 0 \rightarrow 0 \le t \le t_g \\ u_g(t) = u_g \rightarrow t_g < t \le t_f \end{cases}$ $x = 0.45$ m $\Rightarrow P_g = 101375$ Pa
(6)	$t = 0 \Rightarrow Y_{O_2} = 0.204$	$x = 0.00 \Rightarrow Y_{O_2} = 0.204$ $x = 0.45$ m $\Rightarrow -D_g \frac{\partial(\rho_g Y_{O_2})}{\partial x} = h_m(Y_{O_2 0} - Y_{O_2}) \rightarrow h_m = 100$ kg m^{-2} s^{-1}
(7–8)	$t = 0 \Rightarrow T_s = T_g = T_0 = 298$ K	$x = 0.10$ m $\Rightarrow \begin{cases} -k_{eff}\frac{\partial T_s}{\partial x} = 25\ \text{kWm}^{-2} \rightarrow 0 \le t \le t_h \\ -k_{eff}\frac{\partial T_s}{\partial x} = 0 \rightarrow t_h < t \le t_f \\ T_g = 298\ \text{K} \end{cases}$ $x = 0.45$ m $\Rightarrow \begin{cases} -k_{eff}\frac{\partial T_s}{\partial x} = 0 \\ -k_g\frac{\partial T_g}{\partial x} = 0 \end{cases}$

the conservation of mass for solid:

$$\frac{\partial(Y_b)}{\partial t} = -R_b$$
$$\frac{\partial(Y_c)}{\partial t} = v_c R_b - R_c \quad (4)$$

and gas:

$$\frac{\partial(\rho_g \phi_g)}{\partial t} + \frac{\partial(\rho_g u_g)}{\partial x} = (\phi_b \rho_b)((1 - v_c)R_b + (1 - v_{O_2})R_c) \quad (5)$$

phases, where v_c is the char yield coefficient and v_{O2} is the oxygen stoichiometric coefficient. Equation (5) adopts Darcy's Law without gravity effects and the gas density (ρ_g) follows the ideal gas law. A homogeneous porous medium was assumed with intrinsic permeability $k_p = 1 \times 10^{-9}$ m^2 [19] and sand particles were taken as spheres ($A_{s,sp}/V_{sp} = 6(1\text{-}\phi)/d_p$). The bulk transport of oxygen is described by:

$$\phi_g \frac{\partial(\rho_g Y_{O_2})}{\partial t} + \frac{\partial(\rho_g u_g Y_{O_2})}{\partial x} = \phi_g \frac{\partial}{\partial x}\left(\rho_g D_g \frac{\partial Y_{O_2}}{\partial x}\right) - (\phi_b \rho_b) v_{O_2} R_c \quad (6)$$

where the diffusion coefficient $D_g = 4.53 \times 10^{-5}$ m^2 s^{-1} [17]. The model solves the transient energy equation for both solid (representing the combined, effective properties of bitumen plus sand) (T_s) and gas (T_g) phases, respectively:

$$(\rho C_p)_{eff} \frac{\partial T_s}{\partial t} = \frac{\partial}{\partial x}\left(k_{eff} \frac{\partial T_s}{\partial x}\right) - U\left(\frac{A_{s,cl}}{V_{cl}}\right)(T_s - T_0) + h_{sg}\left(\frac{A_{s,sp}}{V_{sp}}\right)(T_g - T_s) - Q \quad (7)$$

$$\phi_g(\rho_g C_{p_g}) \frac{\partial T_g}{\partial t} + \rho_g C_{p_g} u_g \frac{\partial T_g}{\partial x} = \phi_g \frac{\partial}{\partial x}\left(k_g \frac{\partial T_g}{\partial x}\right) + h_{sg}\left(\frac{A_{s,sp}}{V_{sp}}\right)(T_s - T_g) \quad (8)$$

with h_{sg} specified by Eq. (2) unless otherwise indicated. Effective thermal properties for the solid/liquid phases were considered: $(\rho C_p)_{eff} = (1\text{-}\phi)(\rho_s C_{ps}) + (\phi_b)(\rho_b C_{pb})$, $k_{eff} = (1\text{-}\phi)(k_s + k_{rad}) + (\phi_b)(k_b)$, and $\phi = \phi_g + \phi_b$, where total porosity $\phi = 0.37$, liquid-filled porosity $\phi_b = \phi S_b = 0.055$, and gas-filled porosity $\phi_g = 0.315$.

Conduction, convection, and radiation are included with the latter using the Rosseland approximation and expressed as a radiative conductivity ($k_{rad} = 16\sigma d_p T_s^3/3$), with the Stefan–Boltzmann constant $\sigma = 5.67 \times 10^{-8}$ W m^{-2} K^{-4} [19]. Since temperature data are measured at the column center-line, radial heat losses are taken into account via a global heat loss coefficient, U [8], which used the surface area per unit volume ($A_{s,cl}/V_{cl} = 2/r$) of the column, with radius $r = 0.08$ m. The thermal properties of air and sand vary with temperature (see [19] for measurements and details) whereas bitumen specific heat capacity ($C_{pb} = 921$ J kg^{-1} K^{-1} [22]) and thermal conductivity ($k_b = 0.15$ W m^{-1} K^{-1} [23]) are assumed constant. The fuel is considered immobile. The source/sink term (Q) in Eq. (7) is defined as:

$$Q = (\phi_b \rho_b)(\Delta H_c R_c + \Delta H_b R_b) \quad (9)$$

where ΔH_b and ΔH_c can be found in Table 2. The initial and boundary conditions are defined in Table 3. Note that the inlet boundary specifies a constant, positive air mass flux after the air is turned on (time t_g) and the outlet boundary specifies free air exit and zero conduction; as a result, the only means for energy to leave the column is via the heat content of the exiting air.

Three parameters (v_{O2}, v_c, and U) are not independently known, and thus their values were calibrated to experimental results. A sensitivity analysis to all key parameters (not shown) revealed that the calculated A_c produced a non-self-sustaining smouldering front in all cases, which is not realistic. TG heating rates are inevitably smaller than those relevant to smouldering, privileging some minor, low temperature reactions that disappear at high heating rates [1], therefore, affecting the A_c value. Thus, A_c was corrected by treating it as a fourth fitting parameter.

The model calibration involved minimizing the error between the model prediction (*num*) and Exp. #1 (*exp*, average of three repeats) giving equal weight to four aspects of the fit: average peak temperature (T_p), smouldering front velocity (v_f), temperature versus time plots ($T(t)$), and temperature versus distance profiles ($T(x)$):

$$\text{ERROR [\%]} = \frac{1}{4}\left|\frac{T_{p_{exp}} - T_{p_{num}}}{T_{p_{num}}}\right| + \frac{1}{4}\left|\frac{v_{f\,exp} - v_{f\,num}}{v_{f\,num}}\right| + \frac{1}{4}\text{NRMSD}_{T(t)} + \frac{1}{4}\text{NRMSD}_{T(x)} \quad (10)$$

where the average Normalized Root-Mean-Square Deviation (NRMSD) follows the approach taken in [19]. v_f was calculated from the time lapse of the front arrival at two consecutive thermocouples and their known separation distance [6], and a single average value for each experiment was used. The four parameters (A_c, v_{O2}, v_c, and U) were systematically adjusted in following ranges: $U = 5$–16 W m^{-2} K^{-1}, $\log(A_c) = 3$–6 (with 3 being the value obtained from independent experiments (Table 2)), $v_c = 0.4$–0.6, and $v_{O2} = 0.5$–3 kg O$_2$ kg fuel^{-1}. The final choice of $U = 13$ W m^{-2} K^{-1}, $\log(A_c) = 4.9$, $v_c = 0.55$, and $v_{O2} = 1.7$ kg O$_2$ kg fuel^{-1} resulted in the minimum ERROR $= 13 \pm 3\%$.

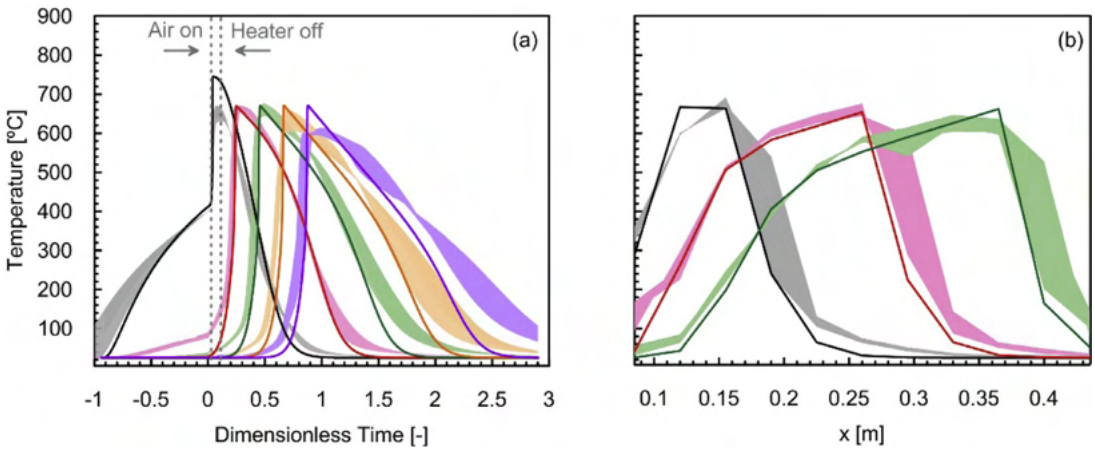

Fig. 2. (a) Temperature evolution versus dimensionless time (DT) and (b) temperature profile versus height of the column (x). The coloured shading encompass three experimental repeats and show (a) thermocouple positions (x) from 0.12 to 0.40 m with 0.07 m intervals and (b) experimental DT = 0.2, 0.5, and 0.8. Solid lines describe the model-predicted sand/bitumen temperature (T_s), plotted at the same DTs (a) and same spatial resolution (b) for comparison purposes.

3. Results

3.1. Model calibration

Figure 2 compares Exp. #1 (three repeats) and the calibrated simulation. The experimental time (t) was normalized, for the purpose of averaging the experiments, and is referred to as Dimensionless Time ($DT = (t\text{-}t_g)v_f/L$ [20]) where $DT < 0$ is the pre-heating period, $DT = 0$ is when the air is turned on and smouldering begins, and $DT = 1$ is when no fuel remains. Excellent agreement for temperature in time and space is observed. The average v_f was 4.16 mm min^{-1} (numerical) and 4.96 ± 0.65 mm min^{-1} (experimental) and the average T_p was 641 ± 11 °C (experimental) and 679 °C (numerical). Small differences are observed at early and late time, which is not surprising since experimental observations indicate edge effects not considered in the model. Note that the abrupt slope changes in Fig. 2(b) are the result of the spatial resolution (0.035 m) of the thermocouples in the experiment and the matching resolution plotted for the numerical data; when the numerical data is plotted at the mesh resolution (0.1 mm), the temperature profiles are smooth (figure not shown).

3.2. Developing confidence in the model

The calibrated model was tested against three additional smouldering experiments (Exp. #2–4, Table 1) without any fitting. Figure 3a presents the temperature-time plots for Exp. #3; this an example representative of the results of the three additional experiments. The predicted bitumen/sand temperatures show excellent agreement in time and space, with ERROR = 9%. Figure 3b compares all four experiments in terms of T_p and v_f. Very good agreement between predicted and observed average T_p and v_f was found. Smouldering front velocity increased linearly with increased air flux, as expected [5]. Small differences in T_p at high air flux and in v_f at low air flux are noted. This is likely due to the model's simple approach to handling the global energy balance. Further work is currently investigating these additional factors, which appear to manifest in cases that approach the limits of smouldering. Nevertheless, the model testing performed provides confidence that this simple model does satisfactorily simulate smouldering front propagation under robust, self-sustaining conditions.

3.3. LTE vs LTNE

Since the difference between gas and solid phase temperatures cannot be easily assessed in experiments, the model is an excellent tool to evaluate the role of LTNE in smouldering scenarios. Using the calibrated model and only changing the h_{sg} correlation, Fig. 4 compares LTE, LTNE–Eq. (1), and LTNE–Eq. (2) to Exp. #1 when the smouldering front was midway along the column. Note that the LTE model replaces Eqs. (7) and (8) with a single temperature equation. In the Figure, the LTE and LTNE–Eq. (1) results overlay each other, indicating that the Wakao et al. [18] correlation predicts h_{sg} sufficiently large that it results in LTE; this was true for all smouldering scenarios modelled in this work (results not shown).

Four regions can be identified in Fig. 4. In Region (I), heat transfer mechanisms increase the temperature of the virgin fuel, but no chemical reactions occur (see Fig. 5). Fig. 4 reveals that the LTE and LTNE–Eq. (1) simulations significantly under-

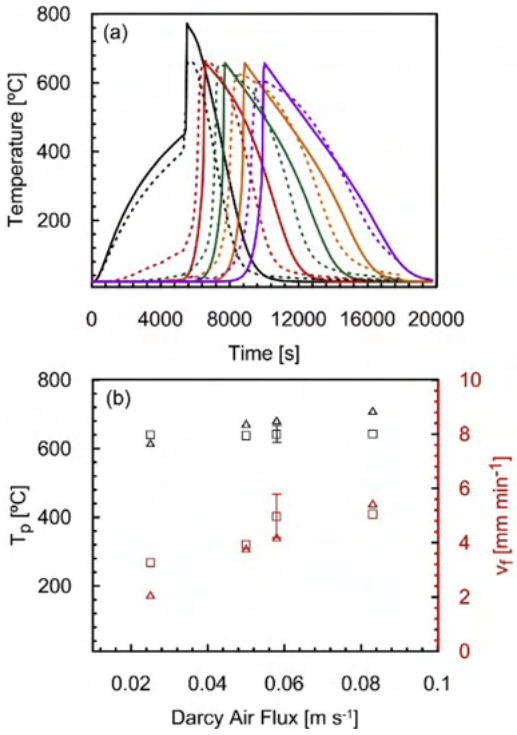

Fig. 3. (a) Temperature vs. time for Exp. #3 ($u_g = 0.05$ m s^{-1}). Dashed lines are experimental data and solid lines are model-predicted sand/bitumen temperature. Colours represent thermocouple positions (x) from 0.12 to 0.40 m with 0.07 m intervals. (b) Peak temperature and smouldering front velocity versus Darcy air flux for all cases: (■) experimental and (▲) numerical data. The error bars denote the variation observed in three repeats of Exp. #1; that simulation was calibrated while the other three were independent.

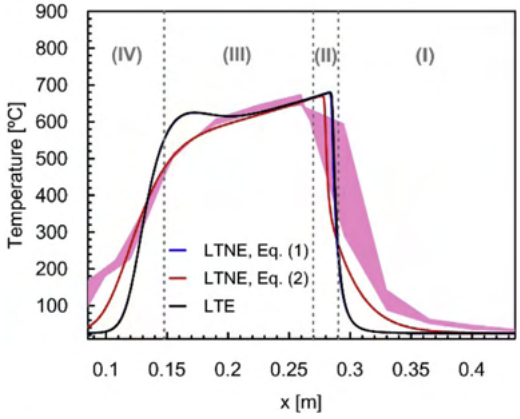

Fig. 4. Temperature profile versus height of the column (x) at DT = 0.5 for Exp. #1. The shading shows experimental data for three repeats. Note that the solid black and blue lines overlay each other. Solid lines are plotted at numerical resolution (mesh size: 0.1 mm). Four distinct regions are identified (see text).

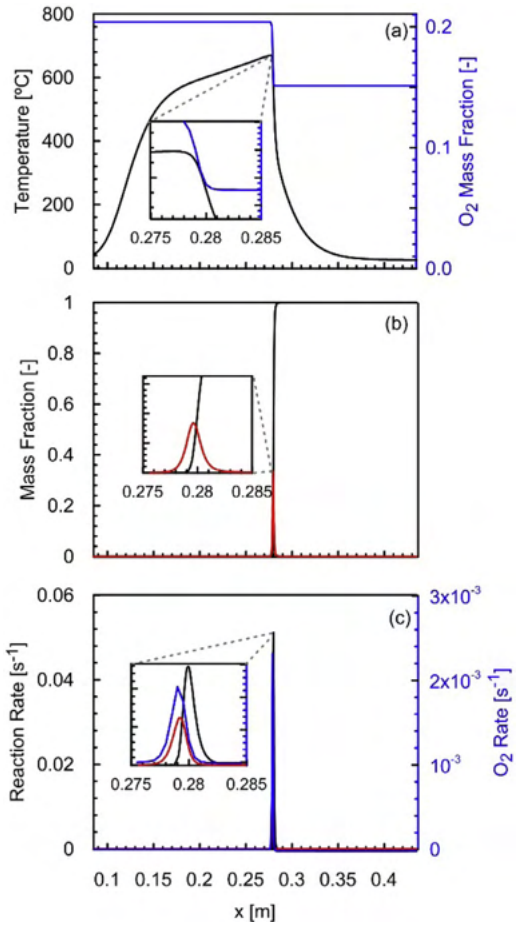

Fig. 5. Model predictions versus height of the column (x) for Exp #1 at DT = 0.5 for: (a) sand/bitumen temperature profile (black) and O_2 mass fraction (blue), (b) mass fractions of bitumen (black) and char (red) and (c) reaction rates for bitumen (black) and char (red), and O_2 consumption rate (blue). These plots correspond to Fig. 4. (For interpretation of the references to color in this figure legend, the reader is referred to the web version of this article.).

predicted temperatures in Region (I), whereas the LTNE–Eq. (2) simulation provides more satisfactory results, with a slower, more realistic spread of the heating front.

Region (II) contains the smouldering front, i.e., where pyrolysis and oxidation reactions occur. Figure 5 confirms that the front is thin, with all the energy absorbed by pyrolysis and released by oxidation located between 0.275 and 0.285 m (Fig. 5c). Correspondingly, all O_2 consumption occurs in this 1 cm front, decreasing from 20.4% to 15.0% (Fig. 5a). Detailed experiments in [3] confirm that smouldering fronts are observed to be on the order of this thickness. Figure 5b shows that within this narrow front, pyrolysis is converting bitumen to char

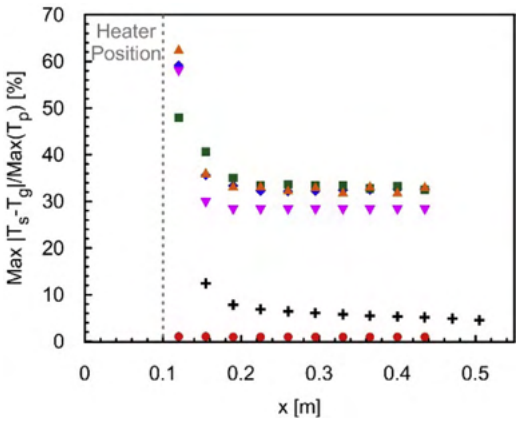

Fig. 6. Normalized maximum difference between model-predicted solid (sand plus bitumen) temperature (T_s) and gas (T_g) temperature varying with column height (x). Smouldering: LTNE–Eq. (2): (■) 0.025 m s^{-1}, (▲) 0.050 m s^{-1}, (♦) 0.058 m s^{-1}, (▼) 0.083 m s^{-1}, and (●) LTNE–Eq. (1), 0.0580 m s^{-1}; Heat Transfer: (+) LTNE–Eq. (2): Exp. *A* from Zanoni et al. [19], 0.089 m s^{-1}.

and then being rapidly oxidized; ultimately, no fuel remained behind the front, which matches all experiments conducted (data not shown). Figure 5c confirms that oxygen consumption is only by oxidation. The excellent prediction of the experiment in this region (Fig. 4) suggests that one oxidation and one pyrolysis reactions are sufficient for predicting the self-sustained smouldering front under robust conditions.

Region (III), located behind the front in Fig. 4, is controlled by the balance between radial heat losses and heat storage by the clean sand. Despite all simulations using the same U (13 W m^{-2} K^{-1}), both LTE and LTNE–Eq. (1) predict the retention of too much heat while LTNE–Eq. (2) more accurately predicts the balance of heat retention, loss, and transfer behind the front. Region (IV) represents the heat transfer between the hot clean sand behind the smouldering front and the cold incoming air. Here too, the LTNE–Eq. (2) model shows the best agreement with experiment, with LTE or LTNE–Eq. (1) simulating extremely fast cooling due to over-predicted interphase heat transfer.

Figure 6 presents the predicted magnitude of LTNE for all simulations. LTNE–Eq. (2) used in the model to predict smouldering conditions (Table 1) showed maximum $\Delta T_{sg}/T_p$ near the heater and decreasing with column height, as expected. The average $\Delta T_{sg}/T_p$ was 36% for air fluxes of 0.025, 0.050, and 0.058 m s^{-1}, and 31% for 0.083 m s^{-1}. This suggests the magnitude of LTNE is significant for smouldering and relatively insensitive to air flux. In contrast, using LTNE–Eq. (1) resulted in predictions of $\Delta T_{sg}/T_p < 1\%$ for the base case (0.058 m s^{-1}), confirming the earlier conclusion that Wakao et al. [18] applied to smouldering predicts essentially LTE conditions.

Figure. 6 also compares Exp. #4 (Table 1) to an identical experiment conducted in [19] except the latter contained no fuel (simply heat transfer in sand by convection). Figure 6 demonstrates that heat transfer in the absence of smouldering exhibits an average $\Delta T_{sg}/T_p = 6\%$, which is more than LTE but less than the smouldering cases. The approximately six times increase in the magnitude of LTNE is not surprising since smouldering oxidation reactions significantly increase temperatures in the fuel/solid phase. This confirms the widely held – but seldom tested – Oliveira and Kaviany [14] assumption that large gradients caused by highly exothermic reactions can create and enhance LTNE conditions.

4. Conclusions

A one-dimensional numerical model of smouldering was developed. It was primarily parameterized with independently measured parameters and, for the remaining four parameters, calibrated against a single, forced air injection, upwards smouldering column experiment containing bitumen mixed with sand. This application represents a soil remediation strategy that is gaining wide acceptance. Confidence in the model was gained by its good predictions of peak temperatures, front velocities, and temperatures in space and time for experiments with different air flow rates.

A relatively simply, two-step kinetic mechanism was found to be sufficient to reproduce the main behaviour of self-sustained smouldering under robust conditions if heat transfer between the phases is treated correctly. LTNE between air and fuel/solid was demonstrated to be significant in smouldering, and incorporating LTNE is clearly important for predicting heat transfer ahead and behind the front during smouldering propagation. Moreover, it was confirmed that the widely employed Wakao et al. [18] correlation essentially predicts LTE and these predictions provide a less accurate match to experiments.

This work represents the first step in developing a model to confidently simulate the wide range of scenarios relevant to liquid smouldering in porous media. Ongoing work is exploring the prediction of smouldering limits and extinction. Nevertheless, it is expected the conclusions presented are widely applicable to smouldering combustion research and applications.

Acknowledgements

Funding was provided by the Ontario Ministry of Research (Grant no. 180804567), Innovation

(Grant no. 341911), and Science as well as the Natural Sciences and Engineering Research Council of Canada (Grant no. RE-WR-01).

References

[1] T.J. Ohlemiller, *Prog. Energy Combust. Sci.* 11 (1985) 277–310.
[2] G. Debenest, V.V. Mourzenko, J.F. Thovert, *Combust. Theory Model.* 9 (2005) 113–135.
[3] M.F. Martins, S. Salvador, J.F. Thovert, G. Debenest, *Fuel* 89 (2010) 133–143.
[4] P. Pironi, C. Switzer, G. Rein, A. Fuentes, J.I. Gerhard, J.L. Torero, *Proc. Combust. Inst.* 32 (2009) 1957–1964.
[5] P. Pironi, C. Switzer, J.I. Gerhard, G. Rein, J.L. Torero, *Environ. Sci. Technol.* 45 (2011) 2980–2986.
[6] C. Switzer, P. Pironi, J.I. Gerhard, G. Rein, J.L. Torero, *Environ. Sci. Technol.* 43 (2009) 5871–5877.
[7] G. Rein, C. Lautenberger, A.C. Fernandez-Pello, J.L. Torero, D.L. Urban, *Combust. Flame* 146 (2006) 95–108.
[8] G. Rein, A. Carlos Fernandez-Pello, D.L. Urban, *Proc. Combust. Inst.* 31 (2007) 2677–2684.
[9] T. Hasan, J.I. Gerhard, R. Hadden, G. Rein, *Fuel* 150 (2015) 288–297.
[10] S.L. MacPhee, J.I. Gerhard, G. Rein, *Environ. Model. Softw.* 31 (2012) 84–98.
[11] H. Fadaei, M. Sennoune, S. Salvador, A. Lapene, G. Debenest, *Fuel* 95 (2012) 197–205.
[12] M.A. Bazelatto Zanoni, H. Massard, M. Ferreira Martins, *Combust. Flame* 159 (2012) 3224–3234.
[13] H.E. Kissinger, *Anal. Chem.* 29 (1957) 1702–1706.
[14] A.A.M. Oliveira, M. Kaviany, *Prog. Energy Combust. Sci.* 27 (2001) 523–545.
[15] X. Huang, G. Rein, H. Chen, *Proc. Combust. Inst.* 35 (2015) 2673–2681.
[16] S.V. Leach, G. Rein, J.L. Ellzey, O.A. Ezekoye, J.L. Torero, *Combust. Flame* 120 (2000) 346–358.
[17] J.L. Torero, A.C. Fernandez-Pello, M. Kitano, *Combust. Sci. Technol.* 91 (1993) 95–117.
[18] N. Wakao, S. Kaguei, T. Funazkri, *Chem. Eng. Sci.* 34 (1979) 325–336.
[19] M.A.B. Zanoni, J.L. Torero, J.I. Gerhard, *Int. J. Heat Mass Transf.* 114 (2017) 90–104.
[20] L. Kinsman, J.L. Torero, J.I. Gerhard, *J. Hazard. Mater.* 325 (2017) 101–112.
[21] K.-Y. Li, X. Huang, C. Fleischmann, G. Rein, J. Ji, *Energy Fuels* 28 (2014) 6130–6139.
[22] R.H. Perry, D.W. Green, Perry's Chemical Engineers' Handbook, 7th ed., McGraw-Hill, New York, USA, 1999, p. 186.
[23] S.K. Elam, I. Tokura, K. Saito, R.A. Altenkirch, *Exp. Therm. Fluid Sci.* 2 (1989) 1–6.